

19 **Abstract**

20 Tropospheric ozone pollution in South Asia is mainly blamed on anthropogenic emissions.
21 However, based on ERA5 reanalysis data, this study highlights the contribution of stratospheric
22 ozone intrusions into the Upper Troposphere and Lower Stratosphere (UTLS) associated with
23 Sudden Stratospheric Warming (SSW) events in enhancing upper tropospheric ozone over the
24 South Asian region. We report an enhancement in ozone in the UTLS by more than 80% for
25 2018 and ~30% within ± 6 days of the onset during SSW events concurrent with the westerly
26 phase of Quasi-biennial oscillation (QBO-SSW) compared to non-SSW years. The
27 equatorward shift (south of 30°N) of the subtropical jet during QBO-SSW causes lowering of
28 the tropopause and more Rossby-wave breaking in the upper troposphere. This results in higher
29 stratospheric ozone intrusions over the South Asian region. The ozone enhancement during
30 QBO-SSW events produces an instantaneous radiative forcing at the top of the atmosphere of
31 $0.09 \pm 0.05 \text{ W.m}^{-2}$ due to UTLS ozone changes and $0.17 \pm 0.05 \text{ W.m}^{-2}$ from total-column ozone
32 changes over South Asia.

33 Keywords: Sudden stratospheric warming, stratosphere intrusions, ozone radiative forcing, South
34 Asian region, Rossby wave breaking.

35

36

37

38

39 1. Introduction

40 Tropospheric ozone is a short-lived greenhouse gas that plays a crucial role in
41 atmospheric chemistry and radiative forcing (Wang et al., 2022). It is also a major air pollutant
42 that significantly affects human health (Lim et al., 2012; Fleming et al., 2018), damages
43 vegetation (Feng et al., 2021), disrupts ecosystems, and imposes economic costs (Dewan and
44 Lakhani, 2022). In South Asia, a significant amount of tropospheric ozone is a growing concern
45 due to its increased hazardous health effects (Lin et al., 2018).

46 The contribution from the downward transport of ozone-rich air from the stratosphere is
47 the largest natural source of tropospheric ozone (e.g., Fadnavis et al., 2010; Roy et al., 2020).
48 Studies have reported that stratospheric influence on the tropospheric ozone exceeds 50% in the
49 winter season at the extratropics (Williams et al., 2019). Wang and Fu (2021) estimate that
50 stratosphere-to-troposphere exchange (STE) contributes approximately 347 ± 12 Tg year⁻¹ to the
51 global tropospheric ozone budget based on both observations and reanalysis data. CMIP6 model
52 simulations for the period 1997 to 2014 indicate that up to 30% of surface ozone in the Northern
53 Hemisphere during winter (DJF) is due to stratospheric ozone intrusions (Li et al., 2024). In the
54 Northwest Pacific, STE increases mid and upper-tropospheric ozone by about 96% in winter and
55 40% in summer between 1990 and 2020 (Ma et al., 2024). Roy et al. (2023) reported an ozone
56 enhancement of ~40 ppb in the upper troposphere over the Indian region caused by stratospheric
57 intrusions associated with tropical cyclones.

58 Sudden stratospheric warming (SSW) events play a key role in atmospheric dynamics
59 and stratospheric ozone intrusions into the troposphere (e.g., Williams et al., 2024). SSWs are
60 one of the most significant large-scale dynamical phenomena in the stratosphere during winter
61 (Butler et al., 2015; Baldwin et al., 2021). Enhanced planetary wave activity from the

62 troposphere disrupts the stratospheric polar vortex, decelerating or even reversing the
63 stratospheric westerlies, and causing a rapid rise in polar stratospheric temperatures by up to 50
64 K within few days (Baldwin et al., 2021). SSW events are crucial in modulating extreme heat, air
65 pollution, wildfires, wind extremes, storm clusters, tropical cyclones, and sea ice melt in the
66 northern high latitudes (Domeisen and Butler, 2020; Domeisen et al., 2020). The temperature
67 and wind anomalies associated with SSWs propagate downward into the troposphere over
68 timescales ranging from weeks to months, impacting tropospheric weather in the Northern
69 Hemisphere for up to 40 days following the onset of the event (Baldwin and Dunkerton, 2001;
70 Hall et al., 2021). Studies also suggest that SSWs are often followed by an equatorward shift of
71 the tropospheric jet stream and storm tracks, as well as surface pressure anomalies that resemble
72 the negative phase of the Northern Annular Mode (Sigmond et al., 2013; Kidston et al., 2015).
73 Projection studies suggest that SSW events will increase by approximately one event per decade
74 by the end of the 21st century (Charlton-Perez et al., 2008). High greenhouse gas emission
75 scenarios indicate a doubling in SSW frequency (Schimanke et al., 2012). Considering the
76 frequent occurrences and the potential role of SSWs in STE, it is important to investigate SSWs
77 influence on tropospheric ozone enhancements and the associated radiative effects.

78 SSW events have a significant influence on STE and impact the tropospheric ozone
79 budget, particularly in high-latitude regions (Xia et al., 2023; Williams et al., 2024; Lee et al.,
80 2025). Based on 11 polar-night jet oscillation (PJO) type SSW events from 1980 to 2013 and
81 chemistry-climate model simulations, STE led to an average increase of 5–10% in near-surface
82 ozone over the Arctic (Williams et al., 2024). Xia et al. (2023) reported an even more
83 pronounced increase of 76% in Arctic surface ozone due to STE in the 2020/21 SSW event.
84 While most of these studies focus on the polar regions, some have identified SSW-induced ozone

85 variability in the mid-latitudes (Liu et al., 2009; Williams et al., 2024). Liu et al. (2009) noted an
86 ozone enhancement of about 186 Tg in the upper troposphere over East Asia during the 2002–
87 2003 SSW, using MOZART-3 simulations. However, tropospheric ozone variations during SSW
88 events over South Asia are among the least studied. Additionally, the broader implications of
89 these events on the ozone radiative forcing over this region remain largely underexplored.

90 In this study, we investigate the impact of all the SSW events from 1962 to 2018 on
91 ozone variability in the upper troposphere and lower stratosphere (UTLS: 300-50 hPa) over the
92 South Asian region (20-35°N, 65-90°E) using ERA5 reanalysis data. The composite is obtained
93 by averaging data with the onset day as a central date (details in the ‘Methods’ section). The
94 February 2018 SSW was a major SSW characterized by pronounced downward propagation of
95 stratospheric signals into the troposphere. It prominently impacted weather across the Northern
96 Hemisphere, including cold extremes over Asia, North America, and Europe (Shi et al., 2023; Lu
97 et al., 2020; Kautz et al., 2020; Xie et al., 2020). Signatures of this event were also seen in ST-
98 Radar observations over India (Ramya et al 2021). ST-Radar observations showed downward
99 propagation of horizontal wind and a pronounced increase of westerly wind amplitude in the
100 UTLS. These findings suggest that the SSW influences the South Asian UTLS. Transport of
101 ozone and ozone radiative forcing due to SSW over South Asia are not investigated yet. Since
102 2018-SSW is a major SSW, and there is evidence of its influence over India (ST-Radar
103 observations), we therefore choose 2018-SSW as a case study, and then extend the analysis to all
104 SSWs and assess their contribution to upper-tropospheric ozone and regional ozone radiative
105 forcing over South Asia.

106 The paper is organised as follows. Section 2 describes the ERA5 reanalysis dataset, and
107 the computation of ozone radiative forcing using the radiative-kernel method. Section 3 presents

108 the (i) UTLS ozone changes during the 2018 SSW event over South Asia, (ii) composite analysis
109 of SSWs, and (iii) ozone radiative forcing. Section 4 summarises the main findings.

110 **2. Methods**

111 **2.1 ERA 5 Reanalysis Data**

112 We analysed daily data of ozone, zonal and meridional winds, geopotential height (GPH),
113 and potential vorticity (PV) from the fifth-generation reanalysis dataset (ERA5) provided by the
114 European Centre for Medium-Range Weather Forecasts (ECMWF) (Hersbach et al., 2020). The
115 ERA5 ozone field is generated through assimilation of multiple satellite- and ground-based
116 observations, including TOMS (1978–2006), SBUV v8.6 (1978–present), CCI MIPAS (2005–
117 2012), SCIAMACHY (2002–2012), Aura MLS v4.2 (2004–present), and OMI-DOAS (2004–
118 present) (Hersbach et al., 2020; S-RIP Final Report, 2022). Comparison of ERA5 ozone with
119 observations shows a slight overestimation in the UTLS. For example, over the North India
120 region, ERA5 shows an overestimation of ~ 20 ppb ozone (Fadnavis et al., 2023). Although
121 ERA5 ozone is biased, it performs better compared to other reanalyses (Fadnavis et al., 2023).
122 The S-RIP (2022) assessment report states an overestimation of zonal mean ozone by ~ 10 – 40%
123 between 50°N and 50°S . The ERA5 variables have a horizontal resolution of $0.25^\circ \times 0.25^\circ$
124 across 37 standard pressure levels (1000 to 1 hPa). Composite analysis is conducted for all
125 variables for ± 30 days, centered on the onset of SSW events (30 days before and after the onset),
126 to assess the impact.

127 The long-term trend is removed from the daily ERA5 data before computing anomalies.
128 This approach ensures that anomalies reflect deviations from typical background conditions. The
129 non-SSW years were first separated into easterly QBO (EQBO-nonSSW) and westerly QBO
130 (WQBO-nonSSW) years. For each non-SSW phase, we applied a Monte Carlo resampling

131 method. For this, calendar-matched non-SSW background samples were constructed by
132 randomly resampling days within the same day-of-year window for the EQBO-nonSSW and
133 WQBO-nonSSW years separately (Dai et al., 2022). In each case, 20,000 random samples of
134 non-SSW episodes were generated. The mean of 20,000 samples for WQBO-nonSSW is referred
135 to as the ‘WQBO-nonSSW climatology’. The same procedure is repeated for the easterly non-
136 SSW phase and is referred to as ‘EQBO-nonSSW climatology’. This climatology was used to
137 calculate composite anomalies for the SSW years (EQBO-SSW – EQBO-nonSSW climatology,
138 WQBO-SSW – WQBO-nonSSW climatology). For the 2018 SSW, which occurred during the
139 westerly QBO phase, we used the ‘WQBO-nonSSW climatology’ for calculating its anomaly.
140 The spread of the 20,000 resampled non-SSW sets for each phase was used to evaluate the
141 statistical significance of the changes caused by the SSWs within that phase (Dai et al., 2022).
142 We then applied an exact Wilcoxon signed-rank test to the same data. A grid point is considered
143 significant only when both tests agree at 95% significance.

144 The onset of all the SSW events is identified as the day when the zonal mean westerly
145 winds at 10 hPa and 60°N reverse their direction from westerlies to easterlies (Charlton and
146 Polvani 2007). Figure S1 shows the temporal evolution of the zonal-mean zonal wind at 60° N
147 and 10 hPa for the 2018 SSW event. To diagnose stratospheric intrusions, we use potential
148 vorticity (PV) as a dynamical tracer of stratospheric air (e.g., Kunz et al., 2011; Holton et al.,
149 1995). Intrusions are identified from PV streamers or tropopause folds when high-PV (≥ 2 PVU)
150 extends equatorward and downward into the upper troposphere (Fig. S2) (e.g., Sprenger et al.,
151 2007). To identify the stratospheric intrusion associated with RWB, we used a criterion of PV >
152 2 PVU and ozone > 80 ppbv at 300 hPa. This criterion is adopted since background ozone at 300
153 hPa is <80 ppbv. To demarcate the tropopause, we used the WMO lapse-rate tropopause (WMO

154 1957). We used the lapse rate tropopause (LRT) derived from the ERA5 data for the present
155 study (Hoffmann and Spand 2022). This definition is adopted to mark a continuous, temporally
156 varying tropopause across the subtropical-tropical transition in our study region. Further, phases
157 of the Quasi-biennial oscillation (QBO) are identified using zonal-mean zonal wind data from
158 radiosonde observations published by the Freie Universität Berlin (Naujokat, 1986). The
159 classification of westerly and easterly QBO phases is based on winds at 70 hPa, over the
160 equatorial latitude band (2°S–2°N). Periods with positive zonal wind values ($>0 \text{ m.s}^{-1}$) are
161 identified as the westerly QBO (WQBO), while periods with negative zonal wind values (<0
162 m.s^{-1}) are classified as the easterly QBO (EQBO).

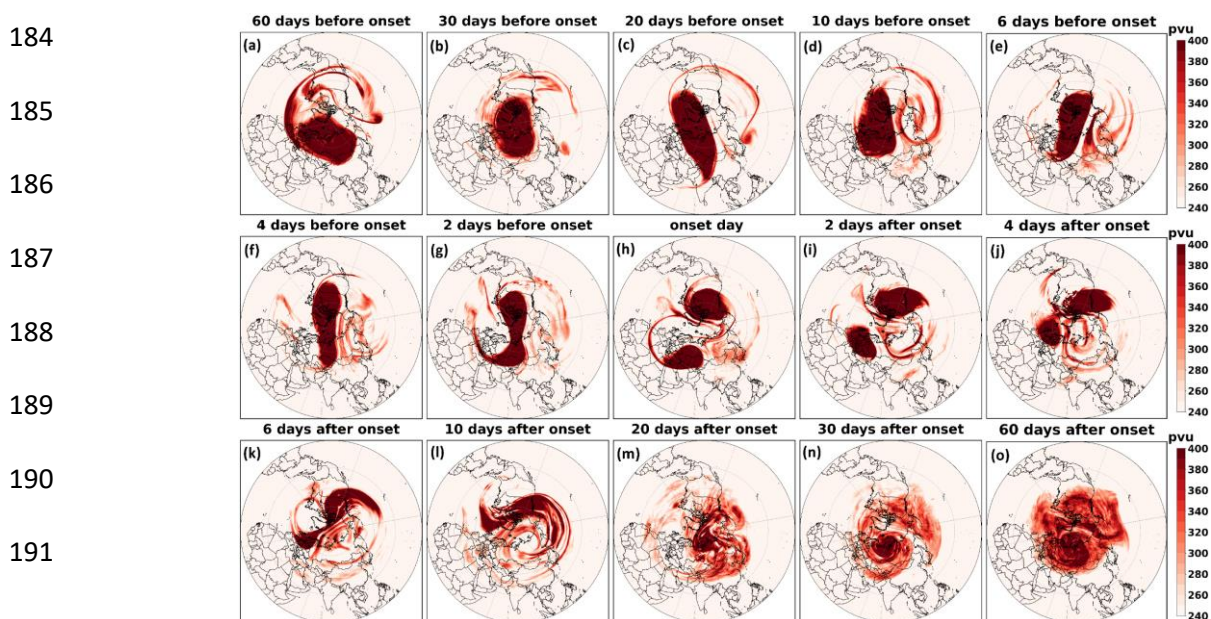
163 **2.2 Computation of ozone radiative forcing**

164 The ozone radiative forcing (RF) is estimated using an ozone radiative kernel method
165 (Skeie et al., 2020). The radiative kernel is constructed using the University of Oslo radiative
166 transfer model (Myhre et al., 2011) by perturbing the ozone layer-by-layer. Temperature, water
167 vapour, and clouds are incorporated into the model from ECMWF's forecast for the year 2003
168 and applied as monthly averages. The model calculates radiative forcing using a broad-band
169 scheme for longwave radiation (Myhre and Stordal, 1997) and the DIScrete Ordinate Radiative
170 Transfer (DISORT) code for shortwave radiation (Stamnes et al., 1988). Previous studies have
171 shown that the ozone radiative forcing estimates from the radiative kernel technique and a
172 radiative transfer model agree within 0.01 W.m^{-2} globally (Iglesias-Suarez et al., 2018). Before
173 applying the kernel, the ERA5 ozone data are linearly interpolated to the kernel resolution ($\sim 5.6^\circ$
174 $\times 5.6^\circ$ horizontal, with 60 vertical levels). The interpolated ozone fields are first converted into
175 layer-wise partial column amounts in Dobson units (DU) following Ziemke et al. (2001). Ozone
176 anomalies in DU are then computed from the non-SSW climatology at each grid point. These

177 layer-wise DU anomalies are multiplied by the long-wave instantaneous clear-sky ozone kernel
 178 ($\text{W}\cdot\text{m}^{-2}\cdot\text{DU}^{-1}$), which gives the change in top-of-atmosphere (TOA) long-wave radiative flux
 179 (defined as an increase in net downward flux; $\Delta (F_{\text{in}} - F_{\text{out}}) > 0$) per DU of ozone change in each
 180 layer. Following Shell et al. (2008), we calculate the instantaneous ozone RF by vertically
 181 summing the layer-wise TOA contributions from the UTLS and the total atmosphere.

182 3. Results

183 3.1 Polar vortex evaluation in 2018 SSW event



192 **Figure 1.** Time slice of the spatial distribution of potential vorticity (PV) at 10 hPa from 60 days
 193 before to 30 days after the onset of the 2018 SSW event.

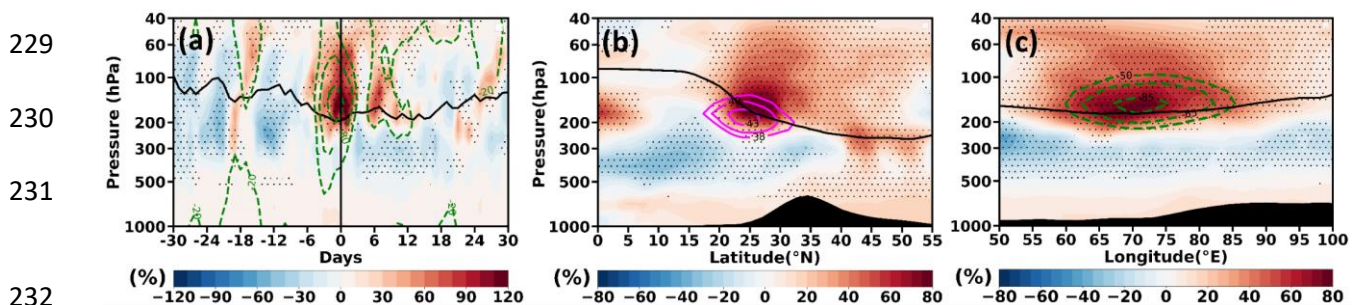
194 The time evolution of the vortex structure depicted by PV at 10 hPa for ± 60 days around
 195 the 2018 SSW onset is shown in Fig. 1. As the SSW event approaches, the vortex begins to
 196 elongate and become asymmetrical (Fig. 1a-g) due to the influence of planetary wave activity
 197 propagating upward from the troposphere; such deformation of the vortex was reported in the
 198 past (e.g., Baldwin et al., 2021). On the onset day (12 February), the vortex splits into two high-
 199 PV lobes, one positioned over North America and another over Eurasia (Fig. 1h). Following the

200 onset, smaller vortices exhibit swirling and filamentation, with the Eurasian lobe drifting
201 westward (Fig. 1i-j). Polar vortex splitting or deformations cause equatorward meandering of
202 upper tropospheric jet that affect the Rossby wave breaking (RWB) and ozone intrusions in the
203 mid-latitudes (Baldwin et al., 2021; Albers et al., 2015). The equatorial meandering of the jet
204 may influence the tropical region; however such analysis is sparse. In the following sections we
205 show the influence of the 2018 SSW on the South Asian region. First we show ozone variation in
206 the UTLS over South Asia and then explain the associated dynamical changes in RWB and the
207 upper tropospheric jet.

208 **3.2 February 2018 SSW case: UTLS ozone variation**

209 Figure 2a shows the vertical distribution of the temporal evolution of ozone anomalies
210 averaged over South Asia for the 2018 SSW event. There is a large ozone enhancement in the
211 UTLS, with values $>80\%$ (>150 ppb) in 2018 within ± 6 days around the SSW onset. Figure 2a
212 indicates that the ozone enhancements in the UTLS region coincide with negative geopotential
213 height (GPH) anomalies. Since the most pronounced ozone enhancement in the UTLS is
214 observed within ± 6 days around the SSW onset, all subsequent analyses in this study are
215 performed for this time period. The latitude–pressure (Fig. 2b) and longitude–pressure (Fig. 2c)
216 cross-sections of ozone anomalies show large ozone enhancement for ± 6 days around the onset
217 in the UTLS over South Asia, exceeding 60% (>80 ppb). Interestingly, a peak in ozone
218 enhancement is seen at the subtropical jet core (Fig.2b). This suggests the role of the subtropical
219 jet causing ozone enhancement in the upper troposphere over South Asia. The strong negative
220 GPH anomaly (indicating a low-pressure area) coincident with large ozone enhancements
221 provides evidence of stratospheric intrusions occurring during the 2018 SSW event (Fig. 2c). In
222 addition, the reduced tropopause height near the onset in Fig.2a shows the occurrence of

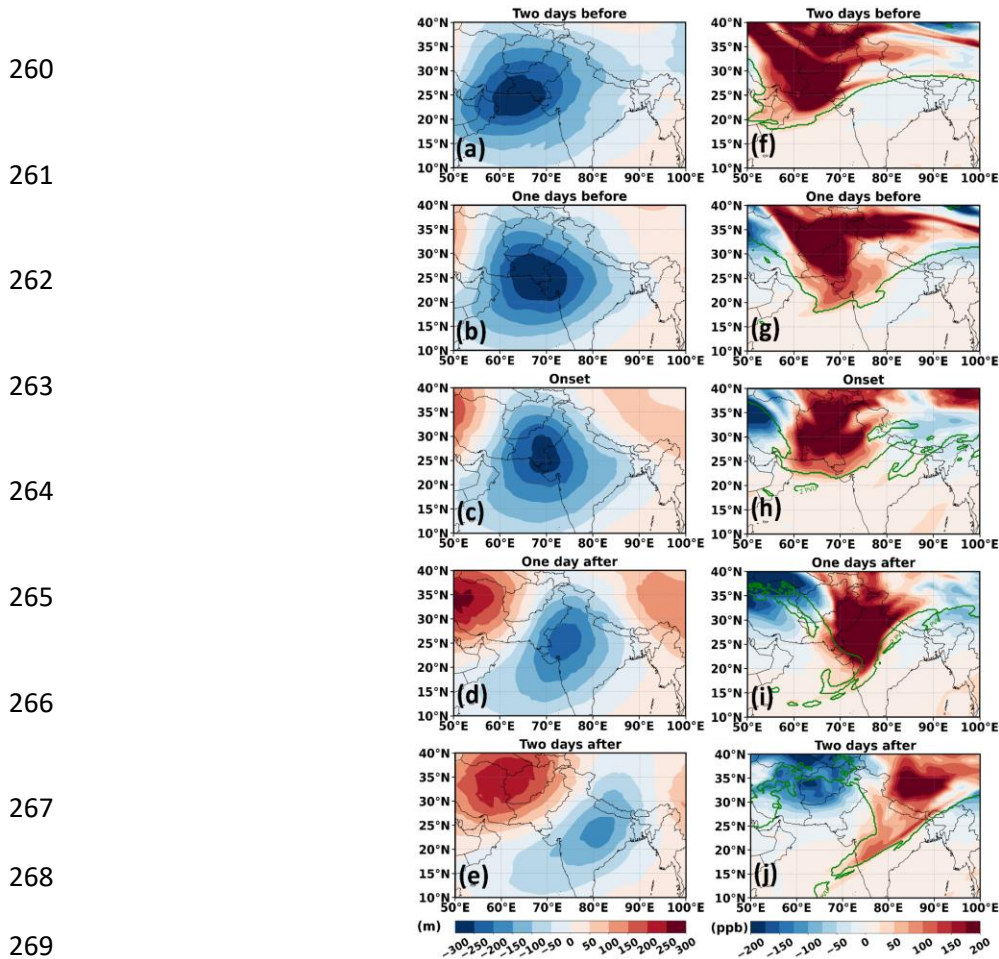
223 tropopause folds. Earlier studies have shown that Rossby wave breaking (RWB) produces
 224 tropopause folds, providing an efficient pathway for quasi-isentropic descent of ozone-rich
 225 stratospheric air into the UTLS (Sprenger et al., 2003; Holton et al., 1995). Past literature reports
 226 ozone enhancements in the polar region associated with SSW (e.g., Baldwin et al., 2021);
 227 however, high ozone enhancement in the UTLS over the South Asian region underscores the
 228 unique regional impacts of SSWs.



233 **Figure 2.** (a) Temporal evolution of vertical ozone anomalies averaged over the South Asian
 234 region (65-90°E, 20-35°N) from 30 days before to 30 days after the onset for the 2018 event. (b)
 235 Latitude-pressure section of ozone anomalies averaged over South Asia (65 - 90°E) for ± 6 days
 236 around the onset for 2018 SSW event. (c) is the same as that of (b) but represents longitude
 237 variations of vertical ozone anomalies averaged over South Asia (20-35°N). The vertical solid
 238 black line in (a) represents the onset day. Magenta solid contour lines in (b) represent the mean
 239 zonal wind and green dashed contour lines in (a) and (c) represent the GPH anomaly. Solid black
 240 lines in panels (a-c) represent the lapse rate tropopause. Black dots indicate a region of 95%
 241 confidence level.

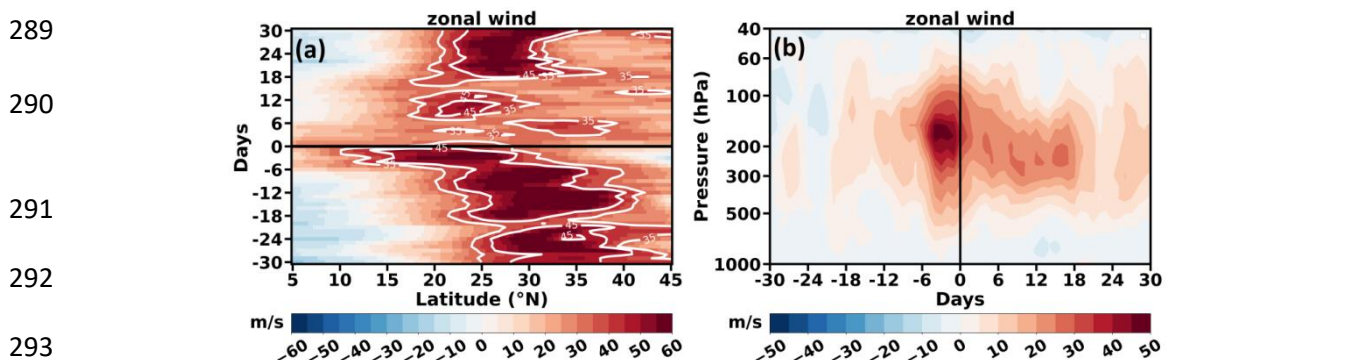
242 Further, we discuss the possible mechanism responsible for the ozone enhancement in the
 243 UTLS over South Asia associated with the 2018 SSW event. Several studies have shown that
 244 SSW-related planetary wave disturbances occur across a deep layer of the stratosphere (e.g.,
 245 Albers et al., 2016). These disturbances extend downward and disrupt horizontal flows in the
 246 upper troposphere (200 hPa) (Albers et al., 2016). To explore the influence of these disturbances
 247 over the South Asian region, we analysed GPH anomalies at 200 hPa. The evolution of GPH
 248 anomalies at 200 hPa for ± 2 days around the SSW onset (Feb. 12, 2018) is shown over the South
 249 Asian region in Fig. 3a-e and for the Northern Hemisphere in (Fig. S3a-e). In the Northern

250 Hemisphere, patterns of high and low GPH anomalies at 200 hPa in the subtropical region (15-
 251 40°N) indicate the presence of synoptic-scale Rossby waves in the upper troposphere (Fig. S3a-
 252 e). The low GPH anomaly over South Asia (also see Fig. 3a-e) indicates a low-pressure area
 253 causing deepening of trough. It is associated with the eastward propagation of Rossby waves,
 254 which can facilitate enhanced stratospheric intrusions. RWB is characterised by large filaments
 255 of high-potential vorticity (PV) air extending towards the equator. The 2 PVU contour lines,
 256 along with ozone anomaly maps at 200 hPa, depicted in Fig. 3f-j show clear indications of RWB
 257 causing ozone intrusions over South Asia. Such quasi-isentropic equatorward excursions cause
 258 irreversible ozone intrusion from the lower stratosphere into the upper troposphere (e.g., Holton
 259 et al., 1995;-Waugh and Polvani, 2000).



270 **Figure 3.** Spatial map of (a-e) GPH anomaly at 200 hPa, (f-j) ozone anomaly at 200 hPa from 2
 271 days before to 2 days after the onset of the 2018 SSW event, along with 2 PVU contour (green
 272 solid line), shown at 1-day intervals.

273 Figures 3f-j clearly show that intrusions near SSW onset days cause large ozone
 274 enhancements >150 ppb ($>80\%$) over South Asia. Since the location and strength of the
 275 subtropical jet set the refractive waveguide and the location of wave breaking (Hoskins &
 276 Ambrizzi 1993; Hitchman & Huesmann 2007), we next diagnose the jet's evolution during this
 277 period. Figure 4 displays the latitude-time Hovmöller diagrams of zonal wind at 200 hPa and the
 278 time-altitude section around the onset over the South Asian region. Figure 4 clearly shows the
 279 equatorward shift of the subtropical jet around onset, creating the background flow conducive to
 280 the RWB and ozone intrusions seen in Fig. 3. The time evolution of zonal winds depicted in
 281 Figure 4a shows that thirty days before the onset, the subtropical jet core is positioned over the
 282 northern part of the Indian subcontinent, and migrates equatorward more prominently for ± 6
 283 days around the onset. The vertical variation of zonal wind (Fig. 4b) also indicates an
 284 equatorward displacement of the subtropical jet, with enhanced westerlies near 200 hPa
 285 extending into $10\text{--}20^\circ\text{N}$ over $65\text{--}90^\circ\text{E}$ around the onset day. Such changes in jet structure are
 286 consistent with a stronger upper-tropospheric Rossby-wave waveguide and background
 287 conditions under which RWB is more likely to occur near the tropopause (Hoskins and Ambrizzi
 288 1993; Homeyer and Bowman 2013).



294 **Figure 4.** (a) Latitude-time plot of zonal wind averaged over South Asia (65° - 90° E) at 200
295 hPa. (b) Time-pressure plot of zonal wind averaged over the South Asian region (65 - 90° E, 10 -
296 20° N) for ± 30 days around the onset of the 2018 SSW event. The horizontal solid line in (a) and
297 the vertical solid line in (b) represent the onset day.

298 The observed equatorward shift of the subtropical jet during the 2018 SSW may also be
299 influenced by the concurrent phase of the Quasi-Biennial Oscillation (QBO) (e.g., White et al.,
300 2016; Li et al., 2023). Notably, the February 2018 SSW took place during the westerly phase of
301 the QBO (Butler et al., 2020). Earlier studies have reported an equatorward shift of the
302 subtropical jet over the East Asia–North Pacific region during the westerly phase of QBO (Park
303 et al., 2021). Our analysis reveals a similar equatorward displacement of the subtropical jet over
304 South Asia during SSWs (Fig. 4a), coinciding with the westerly QBO phase. During the
305 westerly QBO, the associated secondary circulation warms the equatorial lower stratosphere and
306 cools the subtropics, sharpening and shifting the UTLS meridional temperature gradient
307 equatorward (e.g., Hitchman et al., 2021). By thermal-wind balance, this strengthens upper-
308 tropospheric westerlies on the equatorward flank and displaces the subtropical jet equatorward
309 over South Asian longitudes, favouring subtropical wave guidance, RWB, and PV-streamer
310 intrusions (Homeyer & Bowman, 2013; Albers et al., 2016). Additionally, previous studies have
311 shown that the westerly phase of QBO (WQBO) is associated with a lowering of the tropopause
312 (Collimore et al., 2003; Kumar et al., 2014). This lowering perturbs the subtropical waveguide
313 structure and enhances tropopause fold activity (Kumar et al., 2020), thereby increasing the
314 frequency of Rossby wave breaking and strengthening stratosphere–troposphere exchange,
315 causing enhanced ozone intrusions. While these results support a physically plausible role of
316 WQBO in preconditioning the subtropical jet and waveguide over South Asia, the detailed
317 dynamical interaction between the QBO and the SSW that leads to the observed jet shift and
318 enhanced RWB frequency is beyond the scope of present study.

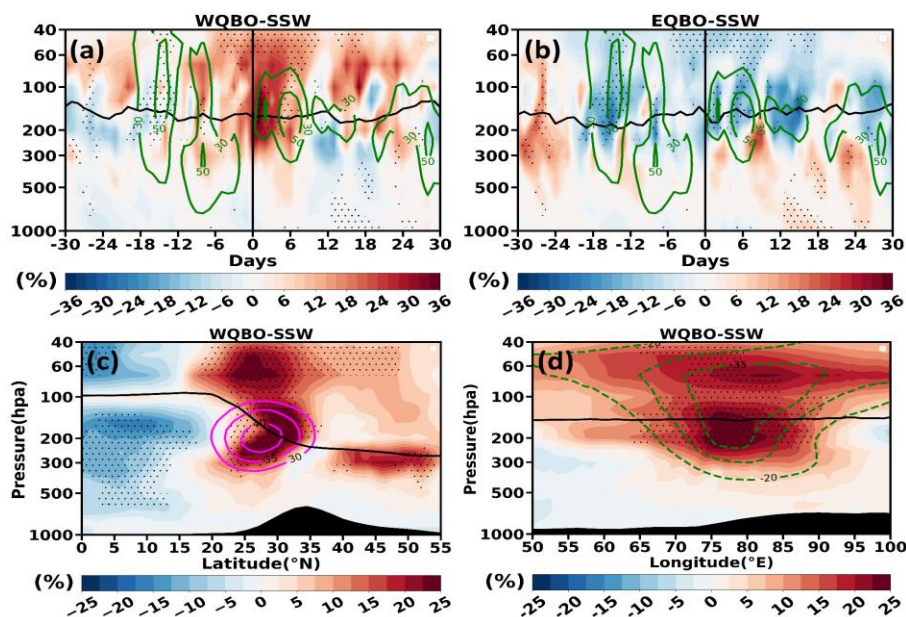
319 3.3 Composite UTLS Ozone Response during all SSW Events

320 Further, we investigate the twenty-seven major SSW events from 1962 to 2017, to
321 examine their influence on ozone variability in the upper troposphere over the South Asian
322 region. Motivated by the 2018 case study, we examined whether the QBO-phase dependence is
323 evident across events. Table 1 lists all the major SSW events considered in this study along with
324 their QBO phases. Of the 27 major SSWs, 15 occur during the westerly phase (WQBO-SSW)
325 and 12 during the easterly phase (EQBO-SSW).

326 **Table 1.** List of all major SSW events from 1962 to 2018 considered for the present analysis
327 alongside their onset dates and QBO phases at 70 hPa.

Year	Onset day	QBO Phase
1963	28 January	Westerly
1966	23 February	Easterly
1968	7 January	Westerly
1969	13 March	Easterly
1970	2 January	Westerly
1971	18 January	Easterly
1973	31 January	Easterly
1977	9 January	Westerly
1979	22 February	Westerly
1980	29 February	Easterly
1981	4 March	Westerly
1984	24 February	Westerly
1985	1 January	Easterly
1987	23 January	Westerly
1988	14 March	Westerly
1989	21 February	Westerly
1999	26 February	Easterly
2000	20 March	Westerly
2001	11 February	Westerly
2003	18 January	Westerly
2004	5 January	Easterly
2006	21 January	Easterly
2007	24 February	Westerly
2008	22 February	Easterly
2009	24 January	Easterly
2010	9 February	Westerly
2013	6 January	Easterly
2018	12 February	Westerly

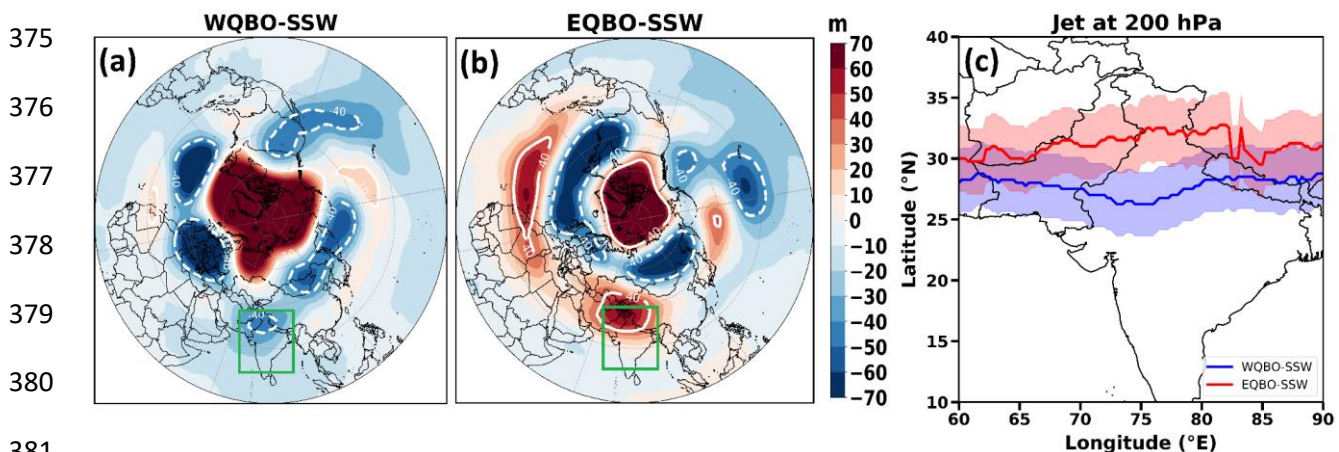
338 Figure 5a shows that, during the composite WQBO-SSW events, ozone intrudes down to
 339 400 hPa, with anomalies exceeding $\sim 30\%$ (over 80 ppb) within ± 6 days of the onset. On the
 340 other hand, during the composite EQBO-SSW events, no significant ozone intrusion is evident
 341 within the same period (Fig. 5b). The latitude–pressure (Fig. 5c) and longitude–pressure (Fig.
 342 5d) sections for WQBO-SSW further reveal enhanced ozone in the UTLS within ± 6 days over
 343 South Asia, with anomalies increases by 20% (>60 ppb) compared to climatology. As seen
 344 earlier (Fig. 2b-c), the maximum ozone enhancement in the WQBO-SSW composite is located
 345 near the subtropical jet core (Fig. 5c) along with a strong negative GPH anomaly (Fig. 5d),
 346 indicating that jet dynamics play a key role in UTLS ozone enhancement during WQBO-SSW.
 347 These enhancements are smaller than in 2018. This may be due to variation in space and time of
 348 ozone intrusions during individual SSW. The averaging across multiple events may subdue the
 349 effect but it remains statistically significant.



356 **Figure 5:** Temporal evolution of vertical ozone anomalies averaged over the South Asian region
 357 ($65\text{-}90^\circ\text{E}$, $20\text{-}35^\circ\text{N}$) from 30 days before to 30 days after the onset for (a) WQBO-SSW and (b)
 358 EQBO-SSW. (c) Latitude–pressure cross-section of ozone anomalies averaged over South Asia
 359 ($65\text{-}90^\circ\text{E}$) for ± 6 days around all the WQBO-SSW onsets. (d) is the same as that of (c) but
 360 represents the longitude variation of vertical ozone anomalies averaged over South Asia (20-

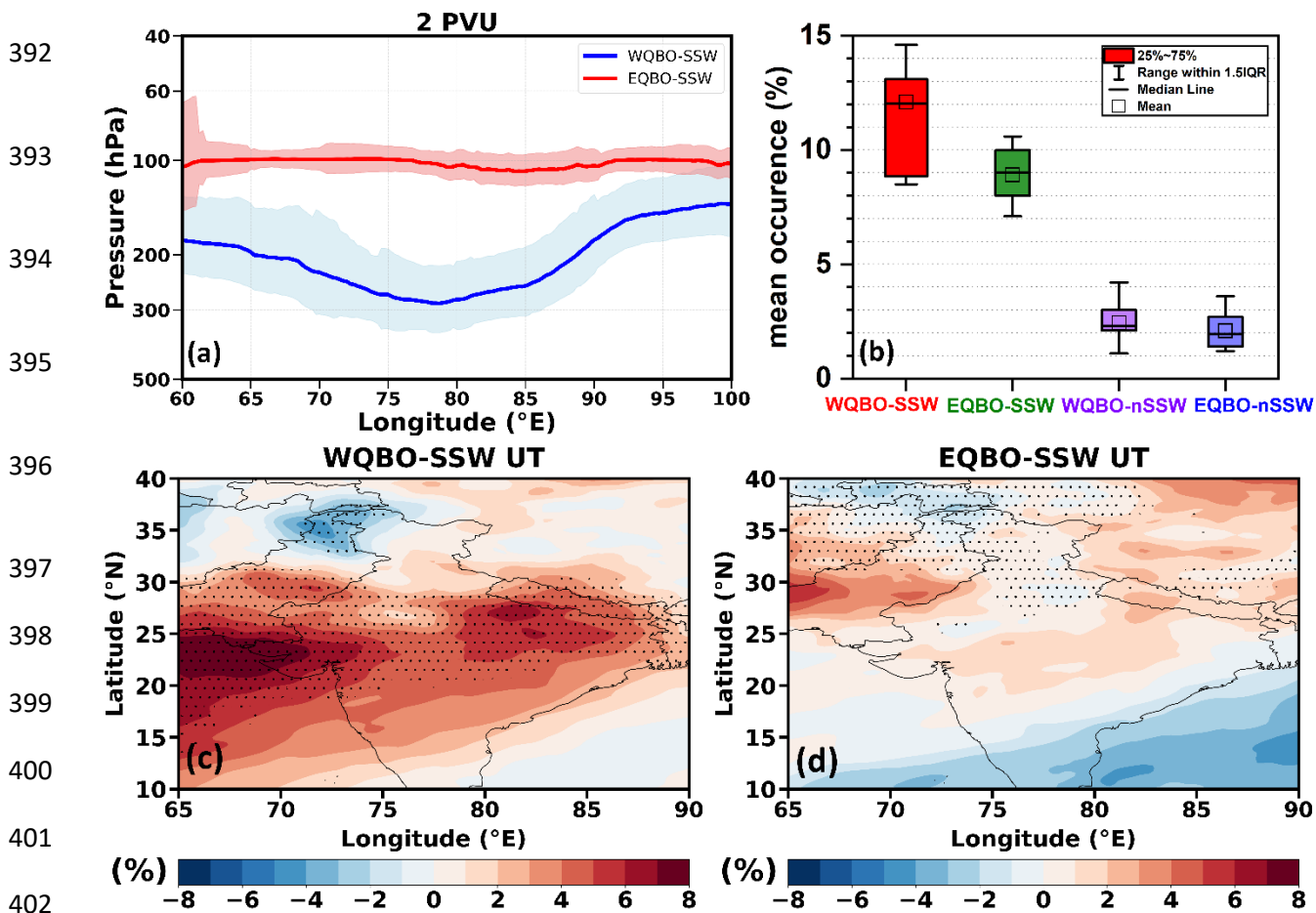
361 35°N). The vertical solid line in (a-b) represents the onset day. Magenta contour lines in (c)
362 represent the mean zonal wind, and dashed green contour lines in (a,d) represent the negative
363 GPH anomaly and solid green contour lines in (b) represent the positive GPH anomaly. Solid
364 black lines in (a-d) represent the lapse rate tropopause. Black dots indicate a region of 95%
365 confidence level.

366 Further, we analysed the GPH anomaly in the upper troposphere for WQBO-SSW and
367 EQBO-SSW composites within ± 6 days around the onset (at 200 hPa) (Figs. 6a–b). The
368 alternating trough–ridge patterns in GPH over the subtropics indicate synoptic-scale Rossby
369 waves in the upper troposphere. During the WQBO-SSW, a pronounced negative GPH anomaly
370 is observed over the South Asian region (Fig. 6a), whereas positive GPH anomalies dominates
371 during the EQBO-SSW (Fig. 6b). The anomalous low over South Asia during WQBO-SSW
372 events indicates a deepening of the upper-tropospheric trough, which favours the tropopause
373 folding and associated stratospheric intrusions into the upper troposphere (e.g., Knowland et al.,
374 2017; Sprenger et al., 2007).



382 **Figure 6.** Spatial map of GPH anomaly for (a) WQBO-SSW and (b) EQBO-SSW and (c) jet
383 core at 200 hPa averaged for ± 6 days around the onset. White solid and dashed contour line in
384 (a-b) indicates positive and negative GPH anomaly. The square box in (a-b) represents the South
385 Asian region considered for the present study. Blue line and red line in (c) represents the jet core
386 for westerly phase and easterly phase of QBO respectively. The shading in (c) represents
387 standard error.

388 Further, we show the position of the subtropical jet core within ± 6 days around the SSW
 389 onset (within ± 6 days) for WQBO-SSW and EQBO-SSW. Figure 6c shows that during WQBO-
 390 SSW, the subtropical jet shifts equatorwardsouth of 30°N . Whereas, during the EQBO-SSW, the
 391 jet (red line) remains north of 30°N . (Detailed mechanism discussed in the section 3.2).



403 **Figure 7.** (a) Longitude-pressure cross section of 2PVU line averaged over South Asia (20-
 404 35°N) for WQBO-SSW and EQBO-SSW composites, shown for the days of deepest intrusion
 405 selected within ± 6 days around the onset. The shading represents standard error. (b) Area-
 406 averaged occurrence frequency (%) of ozone-rich high-PV intrusion signatures consistent with
 407 Rossby wave breaking events during January-March over South Asia identified from $\text{PV} > 2$ and
 408 $\text{Ozone} > 80$ ppbv at 300 hPa for WQBO-SSW, EQBO-SSW, WQBO-nonSSW, and EQBO-
 409 nonSSW. (c) Upper tropospheric ozone anomaly composites (400-250 hPa; in %) for ± 30 days
 410 around onset for WQBO-SSW relative to the corresponding phase-matched non-SSW
 411 climatology WQBO-nonSSW. (d) same as that of (c) but for EQBO-SSW relative to the
 412 corresponding phase-matched non-SSW climatology EQBO-nonSSW. Stippling indicates a
 413 region of 95% confidence level.

414 Figure 7a shows the longitude-pressure cross-section of 2PVU for WQBO–SSW and
415 EQBO–SSW. The figure shows that during the WQBO–SSW, the 2 PVU contour bends
416 downward. While during EQBO–SSW events, the 2 PVU contour remains at higher altitudes,
417 suggesting weaker intrusions. The bending of the 2PVU line is associated with RWB and
418 tropopause folds. We further computed the occurrence frequency of RWB over South Asia for
419 WQBO-SSW, EQBO-SSW, WQBO-nonSSW, and EQBO-nonSSW. Fig 7b shows the highest
420 occurrence of RWB (~12 %) for WQBO-SSW. Upper tropospheric ozone anomalies (400-250
421 hPa) are also highest (~ 8%) for WQBO-SSW (Fig. 7c-d).

422 **3.4 Radiative Forcing of ozone associated with WQBO-SSWs over the South Asian region**

423 Further, we assessed instantaneous radiative forcing at the top of the atmosphere (TOA)
424 due to ozone enhancements in (1) the UTLS and (2) total-column over the South Asian region
425 associated with WQBO-SSW events. The instantaneous RF is computed for ± 6 days around the
426 onset. The estimated RF at the TOA due to the total-column ozone changes is $0.28 \pm 0.19 \text{ W.m}^{-2}$
427 for the 2018 event and $0.17 \pm 0.05 \text{ W.m}^{-2}$ for the composite. These results highlight the
428 significant role of WQBO-SSW events in modulating the radiative balance at the TOA over
429 South Asia. RF at TOA due to the ozone enhancements in the UTLS is $0.25 \pm 0.18 \text{ W.m}^{-2}$ for
430 the 2018 SSW, while the WQBO-SSW composite produces a forcing of $0.09 \pm 0.05 \text{ W.m}^{-2}$. This
431 radiative forcing is due to changes in ozone in the UTLS, where the ozone radiative forcing
432 efficiency is greatest (e.g., Forster and Shine 1997; Ming et al., 2017). These changes in RF can
433 alter local heating rate, temperature, stability, and influence high clouds (e.g., Xia et al., 2018;
434 Nowack et al., 2014).

435

436

437 4. Conclusions

438 Using the ERA5 reanalysis (1962–2018), we investigated the impact of sudden
439 stratospheric warmings (SSWs) on ozone variations in the UTLS (300–50 hPa) over South Asia.
440 Unlike prior global analyses, we demonstrate that SSWs coinciding with the westerly phase of
441 QBO (WQBO-SSW) lead to a substantial enhancement in UTLS ozone and radiative forcing
442 over South Asia. Our analysis shows that the influence of SSW over South Asia is mediated by
443 Rossby-wave dynamics. However, it should be noted that the interaction between the QBO and
444 the SSW leading to the change in the jet and the corresponding RWB breaking is complex. The
445 involved dynamics is beyond the scope of this study.

446 We find that SSWs coinciding with the westerly phase of the QBO (WQBO-SSW) are
447 associated with an equatorward shift of the subtropical jet (south of 30°N) and intensification of
448 RWB. This causes a large ozone enhancement in the UTLS over South Asia (150 ppb (80%) for
449 2018 and 80 ppb (30%) for WQBO-SSW composite). This ozone enhancement in the UTLS
450 during WQBO-SSW events enhances an instantaneous radiative forcing at the top of the
451 atmosphere by $0.25 \pm 0.18 \text{ W.m}^{-2}$ for the 2018 and $0.09 \pm 0.05 \text{ W.m}^{-2}$ during the composite of all
452 WQBO-SSW. The total-column ozone changes enhance the instantaneous RF at the top of the
453 atmosphere increases by $0.28 \pm 0.19 \text{ W.m}^{-2}$ for 2018 and $0.17 \pm 0.05 \text{ W.m}^{-2}$ for the WQBO-
454 SSW composite. This enhancement in TOA radiative forcing does not necessarily imply surface
455 warming, as ozone perturbations can also induce negative surface radiative forcing. For example,
456 Williams et al. (2024) reported a surface forcing of -0.36 W.m^{-2} associated with an increase in
457 ozone in the UTLS. Our radiative kernel method does not estimate a surface forcing associated
458 with ozone changes in the UTLS. The enhancements in ozone and associated RF can affect the

459 stability and temperature of the UTLS, high clouds, and the STE. However, such analysis is
460 beyond the scope of the present study.

461 Since the evolution of the polar vortex modulates the subtropical jet that affects South
462 Asia, these stratospheric influences must be represented in regional prediction systems. Earlier
463 studies have shown that using high-top, stratosphere-resolving models improve subseasonal-to-
464 seasonal predictability (Hardiman et al., 2012; Charlton-Perez et al., 2013; Scaife et al., 2022).
465 We emphasise that models should be extended to the stratosphere, including polar vortex
466 dynamics, for accurate sub seasonal-to-seasonal prediction over South Asia.

467

468 **Code and data availability**

469 The ERA5 data that support the findings of this study are openly available from
470 <https://cds.climate.copernicus.eu/> (<https://doi.org/10.24381/cds.bd0915c6>). All the Figures are
471 created using the Python software. The python code used to plot figures in this paper are
472 available from <https://doi.org/10.5281/zenodo.17639489>

473 **Acknowledgements**

474 The authors thank the staff of the High Power Computing Centre (HPC) in IITM, Pune, India,
475 for providing computer resources and the team members of ERA5 for providing data. The
476 authors are thankful to three anonymous reviewers for their valuable suggestions.

477 **Author contributions**

478 Conceptualisation: S.F. Supervision: SF, MH, RF Investigation and methodology: SC, SR, VS,
479 and PC. Writing: all authors.

480 **Competing interests**

481 At least one of the (co-)authors is a member of the editorial board of Atmospheric Chemistry and
482 Physics.

483 **References:**

484 Albers, J. R., Kiladis, G. N., Birner, T. and Dias, J.: Tropical upper-tropospheric potential
485 vorticity intrusions during sudden stratospheric warmings, *Journal of the Atmospheric*
486 *Sciences*, 73(6), 2361–2384, doi:10.1175/jas-d-15-0238.1, 2016.

487 Baldwin, M. P. and Dunkerton, T. J.: Stratospheric harbingers of anomalous weather regimes,
488 *Science*, 294(5542), 581–584, doi:10.1126/science.1063315, 2001.

489 Baldwin, M. P., Domeisen, D. I. V., Hegglin, M. I., Garny, H., Garfinkel, C. I., Langematz, U.,
490 Charlton-Perez, A. J., Butchart, N., Gerber, E. P., Birner, T., Butler, A. H., Ayarzagüena, B.,
491 and Pedatella, N. M.: Sudden Stratospheric Warmings, *Reviews of Geophysics*, 59,
492 <https://doi.org/10.1029/2020rg000708>, 2021.

493 Butler, A. H., Seidel, D. J., Hardiman, S. C., Butchart, N., Birner, T. and Match, A.: Defining
494 sudden stratospheric warmings, *Bulletin of the American Meteorological Society*, 96(11),
495 1913–1928, doi:10.1175/bams-d-13-00173.1, 2015.

496 Butler, A. H., Lillo, S. P., Long, C. S., Lee, S. H., and Lawrence, Z. D.: Differences between the
497 2018 and 2019 stratospheric polar vortex split events, *Quarterly Journal of the Royal*
498 *Meteorological Society*, 146, 3503–3521, <https://doi.org/10.1002/qj.3858>, 2020.

499 Charlton, A. J. and Polvani, L. M.: A new look at stratospheric sudden warmings. part I:
500 Climatology and modeling benchmarks, *Journal of Climate*, 20(3), 449–469,
501 doi:10.1175/jcli3996.1, 2007.

502 Charlton-Perez, A. J., Polvani, L. M., Austin, J. and Li, F.: The frequency and dynamics of
503 stratospheric sudden warmings in the 21st century, *Journal of Geophysical Research:*
504 *Atmospheres*, 113(D16), doi:10.1029/2007jd009571, 2008.

505 Charlton-Perez, A. J., Baldwin, M. P., Shaw, T. A., Hardiman, S., Polvani, L., Shindell, D.,
506 Yoden, S., Gerber, E. P., Manzini, E., Calvo, N., Yukimoto, S., Lott, F., Davis, N. A., Black,
507 R. X., Butler, A. H., Krüger, K., Son, S., Kim, J., Lee, Y., Mcdaniel, B. A., Reichler, T.,
508 Christiansen, B., Watanabe, S., Toohey, M., Sigmond, M., Gillett, N., Wilcox, L., and
509 Birner, T.: On the lack of stratospheric dynamical variability in low-top versions of the
510 CMIP5 models, *Journal of Geophysical Research: Atmospheres*, 118, 2494–2505,
511 <https://doi.org/10.1002/jgrd.50125>, 2013.

512 Collimore, C. C., Huesmann, A., Martin, D. W., Hitchman, M. H., and Waliser, D. E.: On The
513 Relationship between the QBO and Tropical Deep Convection, *Journal of Climate*, 16,
514 2552–2568, [https://doi.org/10.1175/1520-0442\(2003\)016<2552:otrbtq>2.0.co;2](https://doi.org/10.1175/1520-0442(2003)016<2552:otrbtq>2.0.co;2), 2003.

515 Dai, Y., Hitchcock, P., Mahowald, N. M., Domeisen, D. I., Hamilton, D. S., Li, L., Marticorena,
516 B., Kanakidou, M., Mihalopoulos, N., & Aboagye-Okyere, A. (2022). Stratospheric impacts
517 on dust transport and air pollution in West Africa and the Eastern Mediterranean. *Nature*
518 *Communications*, 13(1). <https://doi.org/10.1038/s41467-022-35403-1>

519 Dewan, S. and Lakhani, A.: Tropospheric ozone and its natural precursors impacted by climatic
520 changes in emission and dynamics, *Frontiers in Environmental Science*, 10,
521 doi:10.3389/fenvs.2022.1007942, 2022.

522 Domeisen, D. I. and Butler, A. H.: Stratospheric drivers of extreme events at the Earth’s surface,
523 *Communications Earth & Environment*, 1(1), doi:10.1038/s43247-020-00060-z, 2020.

524 Domeisen, D. I., Grams, C. M. and Papritz, L.: The role of North Atlantic–European weather
525 regimes in the surface impact of sudden stratospheric warming events, *Weather and Climate*
526 *Dynamics*, 1(2), 373–388, doi:10.5194/wcd-1-373-2020, 2020.

527 Fadnavis, S., Chakraborty, T., and Beig, G.: Seasonal stratospheric intrusion of ozone in the
528 upper troposphere over India, *Annales Geophysicae*, 28, 2149–2159,
529 <https://doi.org/10.5194/angeo-28-2149-2010>, 2010.

530 Fadnavis, S., Wienhold, F. G., Müller, R., Oelsner, P., Vogel, B., Naja, M., Sonbawne, S.,
531 Dirksen, R., Sagalgile, A., and Peter, T.: Comparison of ozonesonde measurements in the
532 upper troposphere and lower Stratosphere in Northern India with reanalysis and chemistry-
533 climate-model data, *Scientific Reports*, 13, <https://doi.org/10.1038/s41598-023-34330-5>,
534 2023.

535 Feng, Z., Agathokleous, E., Yue, X., Oksanen, E., Paoletti, E., Sase, H., Gandin, A., Koike, T.,
536 Calatayud, V., Yuan, X., Liu, X., De Marco, A., Jolivet, Y., Kontunen-Soppela, S., Hoshika,
537 Y., Saji, H., Li, P., Li, Z., Watanabe, M. and Kobayashi, K.: Emerging challenges of ozone
538 impacts on Asian plants: Actions are needed to protect ecosystem health, *Ecosystem Health*
539 *and Sustainability*, 7(1), doi:10.1080/20964129.2021.1911602, 2021.

540 Fleming, Z. L., Doherty, R. M., von Schneidmesser, E., Malley, C. S., Cooper, O. R., Pinto, J.
541 P., Colette, A., Xu, X., Simpson, D., Schultz, M. G., Lefohn, A. S., Hamad, S., Moolla, R.,
542 Solberg, S. and Feng, Z.: Tropospheric Ozone Assessment Report: Present-day ozone
543 distribution and trends relevant to human health, *Elementa: Science of the Anthropocene*, 6,
544 doi:10.1525/elementa.273, 2018.

545 Hall, R. J., Mitchell, D. M., Seviour, W. J. and Wright, C. J.: Tracking the stratosphere-to-
546 surface impact of sudden stratospheric warmings, *Journal of Geophysical Research:*
547 *Atmospheres*, 126(3), doi:10.1029/2020jd033881, 2021.

548 Hardiman, S. C., Butchart, N., Hinton, T. J., Gray, L. J., and Osprey, S. M.: The Effect of a
549 Well-Resolved Stratosphere on Surface Climate: Differences between CMIP5 Simulations
550 with High and Low Top Versions of the Met Office Climate Model, *Journal of Climate*, 25,
551 7083–7099, <https://doi.org/10.1175/jcli-d-11-00579.1>, 2012.

552 Hersbach, H., Bell, B., Berrisford, P., Hirahara, S., Horányi, A., Muñoz-Sabater, J., Nicolas, J.,
553 Peubey, C., Radu, R., Schepers, D., Simmons, A., Soci, C., Abdalla, S., Abellan, X.,
554 Balsamo, G., Bechtold, P., Biavati, G., Bidlot, J., Bonavita, M., De Chiara, G., Dahlgren, P.,
555 Dee, D., Diamantakis, M., Dragani, R., Flemming, J., Forbes, R., Fuentes, M., Geer, A.,
556 Haimberger, L., Healy, S., Hogan, R. J., Hólm, E., Janisková, M., Keeley, S., Laloyaux, P.,
557 Lopez, P., Lupu, C., Radnoti, G., de Rosnay, P., Rozum, I., Vamborg, F., Villaume, S. and
558 Thépaut, J.: The ERA5 global reanalysis, *Quarterly Journal of the Royal Meteorological*
559 *Society*, 146(730), 1999–2049, doi:10.1002/qj.3803, 2020.

560 Hitchman, M. H. and Huesmann, A. S.: A Seasonal Climatology of Rossby Wave Breaking in
561 the 320–2000-K Layer, *Journal of the Atmospheric Sciences*, 64, 1922–1940,
562 <https://doi.org/10.1175/jas3927.1>, 2007.

563 Hitchman, M. H., Tegtmeier, S., Yoden, S., Haynes, P. H., and Kumar, V.: An Observational
564 History of the Direct Influence of the Stratospheric Quasi-biennial Oscillation on the
565 Tropical and Subtropical Upper Troposphere and Lower Stratosphere, *Journal of the*
566 *Meteorological Society of Japan. Ser. II*, 99, 239–267, [https://doi.org/10.2151/jmsj.2021-](https://doi.org/10.2151/jmsj.2021-012)
567 012, 2021.

568 Hoffmann, L. and Spang, R.: An assessment of tropopause characteristics of the ERA5 and era-
569 interim meteorological reanalyses, *Atmospheric Chemistry and Physics*, 22(6), 4019–4046,
570 doi:10.5194/acp-22-4019-2022, 2022.

571 Holton, J. R., Haynes, P. H., McIntyre, M. E., Douglass, A. R., Rood, R. B. and Pfister, L.:
572 Stratosphere-Troposphere exchange, *Reviews of Geophysics*, 33(4), 403–439,
573 doi:10.1029/95rg02097, 1995.

574 Homeyer, C. R. and Bowman, K. P.: Rossby Wave Breaking and Transport between the Tropics
575 and Extratropics above the Subtropical Jet, *Journal of the Atmospheric Sciences*, 70, 607–
576 626, <https://doi.org/10.1175/jas-d-12-0198.1>, 2013.

577 Hoskins, B. J. and Ambrizzi, T.: Rossby Wave Propagation on a Realistic Longitudinally
578 Varying Flow, *Journal of the Atmospheric Sciences*, 50, 1661–1671,
579 [https://doi.org/10.1175/1520-0469\(1993\)050<1661:rwpoar>2.0.co;2](https://doi.org/10.1175/1520-0469(1993)050<1661:rwpoar>2.0.co;2), 1993.

580 Iglesias-Suarez, F., Kinnison, D. E., Rap, A., Maycock, A. C., Wild, O. and Young, P. J.: Key
581 drivers of ozone change and its radiative forcing over the 21st century, *Atmospheric*
582 *Chemistry and Physics*, 18(9), 6121–6139, doi:10.5194/acp-18-6121-2018, 2018.

583 Kautz, L., Polichtchouk, I., Birner, T., Garny, H., & Pinto, J. G. (2020). Enhanced extended-
584 range predictability of the 2018 late-Winter Eurasian cold spell due to the stratosphere.
585 *Quarterly Journal of the Royal Meteorological Society*, 146(727), 1040–1055.
586 <https://doi.org/10.1002/qj.3724>.

587 Kidston, J., Scaife, A. A., Hardiman, S. C., Mitchell, D. M., Butchart, N., Baldwin, M. P. and
588 Gray, L. J.: Stratospheric influence on tropospheric jet streams, storm tracks and Surface
589 Weather, *Nature Geoscience*, 8(6), 433–440, doi:10.1038/ngeo2424, 2015.

590 Kim, J., Park, H.-S., Son, S.-W., and Gerber, E. P.: Defining Sudden Stratospheric Warming in
591 Climate Models: Accounting for Biases in Model Climatologies, *Journal of Climate*, 30,
592 5529–5546, <https://doi.org/10.1175/jcli-d-16-0465.1>, 2017.

593 Knowland, K. E., Ott, L. E., Duncan, B. N. and Wargan, K.: Stratospheric intrusion-influenced
594 ozone air quality exceedances investigated in the NASA Merra-2 Reanalysis, *Geophysical*
595 *Research Letters*, 44(20), doi:10.1002/2017gl074532, 2017.

596 Kumar, V., Dhaka, S. K., Reddy, K. K., Gupta, A., Prasad, S. B. S., Panwar, V., Singh, N., Ho,
597 S.-P., and Takahashi, M.: Impact of quasi-biennial oscillation on the inter-annual variability
598 of the tropopause height and temperature in the tropics: A study using
599 COSMIC/FORMOSAT-3 observations, *Atmospheric Research*, 139, 62–70,
600 <https://doi.org/10.1016/j.atmosres.2013.12.014>, 2014.

601 Kumar, K. N., Sharma, S. K., Naja, M., and Phanikumar, D. V.: A Rossby wave breaking-
602 induced enhancement in the tropospheric ozone over the Central Himalayan region,
603 *Atmospheric Environment*, 224, 117356, <https://doi.org/10.1016/j.atmosenv.2020.117356>,
604 2020.

605 Kunz, A., Konopka, P., Müller, R. and Pan, L. L.: Dynamical tropopause based on isentropic
606 potential vorticity gradients, *Journal of Geophysical Research*, 116(D1),
607 doi:10.1029/2010jd014343, 2011.

608 Lee, J., Butler, A. H., Albers, J. R., Wu, Y. and Lee, S. H.: Impact of sudden stratospheric
609 warmings on the stratosphere-to-troposphere transport of ozone, *Geophysical Research*
610 *Letters*, 52(2), doi:10.1029/2024gl112588, 2025.

- 611 Li, H., Fan, Y., Li, Q., Ji, X., Zhang, J., and Sheng, B.: The Gravity Wave Activity during Two
612 Recent QBO Disruptions Revealed by U.S. High-Resolution Radiosonde Data, Remote
613 Sensing, 15, 472, <https://doi.org/10.3390/rs15020472>, 2023.
- 614 Li, Y., Xia, Y., Xie, F. and Yan, Y.: Influence of stratosphere-troposphere exchange on long-
615 term trends of surface ozone in CMIP6, Atmospheric Research, 297, 107086,
616 doi:10.1016/j.atmosres.2023.107086, 2024.
- 617 Lim, S. S., Vos, T., Flaxman, A. D., Danaei, G., Shibuya, K., Adair-Rohani, H., AlMazroa, M.
618 A., Amann, M., Anderson, H. R., Andrews, K. G., Aryee, M., Atkinson, C., Bacchus, L. J.,
619 Bahalim, A. N., Balakrishnan, K., Balmes, J., Barker-Collo, S., Baxter, A., Bell, M. L.,
620 Blore, J. D., Blyth, F., Bonner, C., Borges, G., Bourne, R., Boussinesq, M., Brauer, M.,
621 Brooks, P., Bruce, N. G., Brunekreef, B., Bryan-Hancock, C., Bucello, C., Buchbinder, R.,
622 Bull, F., Burnett, R. T., Byers, T. E., Calabria, B., Carapetis, J., Carnahan, E., Chafe, Z.,
623 Charlson, F., Chen, H., Chen, J. S., Cheng, A. T.-A., Child, J. C., Cohen, A., Colson, K. E.,
624 Cowie, B. C., Darby, S., Darling, S., Davis, A., Degenhardt, L., Dentener, F., Des Jarlais, D.
625 C., Devries, K., Dherani, M., Ding, E. L., Dorsey, E. R., Driscoll, T., Edmond, K., Ali, S. E.,
626 Engell, R. E., Erwin, P. J., Fahimi, S., Falder, G., Farzadfar, F., Ferrari, A., Finucane, M. M.,
627 Flaxman, S., Fowkes, F. G., Freedman, G., Freeman, M. K., Gakidou, E., Ghosh, S.,
628 Giovannucci, E., Gmel, G., Graham, K., Grainger, R., Grant, B., Gunnell, D., Gutierrez, H.
629 R., Hall, W., Hoek, H. W., Hogan, A., Hosgood, H. D., Hoy, D., Hu, H., Hubbell, B. J.,
630 Hutchings, S. J., Ibeanusi, S. E., Jacklyn, G. L., Jasrasaria, R., Jonas, J. B., Kan, H., Kanis, J.
631 A., Kassebaum, N., Kawakami, N., Khang, Y.-H., Khatibzadeh, S., Khoo, J.-P., et al.: A
632 comparative risk assessment of burden of disease and injury attributable to 67 risk factors
633 and risk factor clusters in 21 regions, 1990–2010: A systematic analysis for the global
634 burden of disease study 2010, The Lancet, 380(9859), 2224–2260, doi:10.1016/s0140-
635 6736(12)61766-8, 2012.
- 636 Lin, Y., Jiang, F., Zhao, J., Zhu, G., He, X., Ma, X., Li, S., Sabel, C. E. and Wang, H.: Impacts
637 of O₃ on premature mortality and crop yield loss across China, Atmospheric Environment,
638 194, 41–47, doi:10.1016/j.atmosenv.2018.09.024, 2018.
- 639 Liu, Y., Gao, S. T., Brasseur, G., Tie, X. X., Wang, H. P., Kinnison, D., and Liu, C. X.:
640 Atmospheric tracers during the 2003–2004 stratospheric warming event and impact of ozone
641 intrusions in the troposphere, Atmospheric Chemistry and Physics, 9, 2157–2170,
642 <https://doi.org/10.5194/acp-9-2157-2009>, 2009.
- 643 Lü, Z., Li, F., Orsolini, Y. J., Gao, Y., & He, S. (2020). Understanding of European cold
644 extremes, sudden stratospheric warming, and siberian snow accumulation in the winter of
645 2017/18. Journal of Climate, 33(2), 527–545. <https://doi.org/10.1175/jcli-d-18-0861.1>

646 Ma, X., Huang, J., Hegglin, M., Joeckel, P. and Zhao, T.: Causes of growing middle-upper
647 tropospheric ozone over the Northwest Pacific Region, doi:10.5194/egusphere-2023-2411,
648 2024.

649 Myhre, G., & Stordal, F.: Role of spatial and temporal variations in the computation of radiative
650 forcing and GWP. *Journal of Geophysical Research: Atmospheres*, 102(D10), 11181–11200.
651 <https://doi.org/10.1029/97jd00148>, 1997.

652 Myhre, G., Shine, K. P., Rädcl, G., Gauss, M., Isaksen, I. S. A., Tang, Q., Prather, M. J.,
653 Williams, J. E., van Velthoven, P., Dessens, O., Koffi, B., Szopa, S., Hoor, P., Grewe, V.,
654 Borken-Kleefeld, J., Berntsen, T. K. and Fuglestvedt, J. S.: Radiative forcing due to changes
655 in ozone and methane caused by the transport sector, *Atmospheric Environment*, 45(2), 387–
656 394, doi:10.1016/j.atmosenv.2010.10.001, 2011.

657 Naujokat, B. (1986). An update of the observed quasi-biennial oscillation of the stratospheric
658 winds over the Tropics. *Journal of the Atmospheric Sciences*, 43(17), 1873–1877.
659 [https://doi.org/10.1175/1520-0469\(1986\)043<1873:auotoq>2.0.co;2](https://doi.org/10.1175/1520-0469(1986)043<1873:auotoq>2.0.co;2).

660 Nowack, P. J., Luke Abraham, N., Maycock, A. C., Braesicke, P., Gregory, J. M., Joshi, M. M.,
661 Osprey, A. and Pyle, J. A.: A large ozone-circulation feedback and its implications for
662 global warming assessments, *Nature Climate Change*, 5(1), 41–45,
663 doi:10.1038/nclimate2451, 2014.

664 Park, C., Choi, J., Son, S., and Lim, Y.: Quasi-biennial oscillation-related surface air temperature
665 change over the western North Pacific in late winter, *International Journal of Climatology*,
666 42, 4351–4359, <https://doi.org/10.1002/joc.7470>, 2021.

667 Remya, R., Manoj, M. G., Rakesh, V., Mohanakumar, K., & Sivan, C. (2021). Influence of high
668 latitude sudden stratospheric warming on tropical weather: Observations from a 205 MHz
669 stratosphere troposphere radar and surface meteorological parameters. *Earth and Space
670 Science*, 8(4). <https://doi.org/10.1029/2020ea001418>.

671 Remya, R., Manoj, M. G., and Mohanakumar, K.: Role of Quasi-Biennial oscillation on the link
672 between sudden stratospheric warming and tropical weather events, *Advances in Space
673 Research*, 73, 571–584, <https://doi.org/10.1016/j.asr.2023.11.006>, 2023.

674 Roy, C., Thazhe Purayil, S., and Fadnavis, S.: The stratospheric ozone rich cold intrusion during
675 El-Nino over the Indian region: implication during the Indian summer monsoon,
676 <https://doi.org/10.5194/egusphere-egu2020-937>, 2020.

677 Roy, C., Ravishankara, A. R., Newman, P. A., David, L. M., Fadnavis, S., Rathod, S. D., Lait,
678 L., Krishnan, R., Clark, H. and Sauvage, B.: Estimation of stratospheric intrusions during

679 Indian Cyclones, *Journal of Geophysical Research: Atmospheres*, 128(3),
680 doi:10.1029/2022jd037519, 2023.

681 Scaife, A. A., Charlton-Perez, A. J., Son, S.-W., Hardiman, S. C., Polvani, L., Lim, E.-P.,
682 Haynes, P., Baldwin, M. P., Shepherd, T. G., Perlwitz, J., Richter, J. H., Noguchi, S.,
683 Thompson, D. W. J., Karpechko, A. Y., Butler, A. H., Scinocca, J., Sigmund, M., Domeisen,
684 D. Shil. V., and Garfinkel, C. I.: Long-range prediction and the stratosphere, *Atmospheric
685 Chemistry and Physics*, 22, 2601–2623, <https://doi.org/10.5194/acp-22-2601-2022>, 2022.

686 Schimanke, S., Spanghel, T., Huebener, H. and Cubasch, U.: Variability and trends of major
687 stratospheric warmings in simulations under constant and increasing GHG concentrations,
688 *Climate Dynamics*, 40(7–8), 1733–1747, doi:10.1007/s00382-012-1530-x, 2012.

689 Shell, K. M., Kiehl, J. T. and Shields, C. A.: Using the radiative kernel technique to calculate
690 climate feedbacks in NCAR’s community atmospheric model, *Journal of Climate*, 21(10),
691 2269–2282, doi:10.1175/2007jcli2044.1, 2008.

692 Shi, Y., Evtushevsky, O., Milinevsky, G., Wang, X., Klekociuk, A., Han, W., Grytsai, A., Wang,
693 Y., Wang, L., Novosyadlyj, B., and Andrienko, Y.: Impact of the 2018 major sudden
694 stratospheric warming on weather over the midlatitude regions of Eastern Europe and East
695 Asia, *Atmospheric Research*, 297, 107112, <https://doi.org/10.1016/j.atmosres.2023.107112>,
696 2023.

697 Sigmund, M., Scinocca, J. F., Kharin, V. V. and Shepherd, T. G.: Enhanced seasonal forecast
698 skill following stratospheric sudden warmings, *Nature Geoscience*, 6(2), 98–102,
699 doi:10.1038/ngeo1698, 2013.

700 Skeie, R. B., Myhre, G., Hodnebrog, Ø., Cameron-Smith, P. J., Deushi, M., Hegglin, M. I.,
701 Horowitz, L. W., Kramer, R. J., Michou, M., Mills, M. J., Olivié, D. J., Connor, F. M.,
702 Paynter, D., Samset, B. H., Sellar, A., Shindell, D., Takemura, T., Tilmes, S. and Wu, T.:
703 Historical total ozone radiative forcing derived from CMIP6 simulations, *npj Climate and
704 Atmospheric Science*, 3(1), doi:10.1038/s41612-020-00131-0, 2020.

705 SPARC Reanalysis Intercomparison Project (S-RIP) Final Report. M. Fujiwara, G.L. Manney,
706 L.J. Gray, and J.S. Wright (Eds.), SPARC Report No. 10, WCRP-17/2020, doi:
707 10.17874/800dee57d13, available at www.sparc-climate.org/publications/sparc-reports,
708 2022.

709 Sprenger, M., Croci Maspoli, M. and Wernli, H.: Tropopause folds and cross-Tropopause
710 Exchange: A global investigation based upon ECMWF analyses for the time period March
711 2000 to February 2001, *Journal of Geophysical Research: Atmospheres*, 108(D12),
712 doi:10.1029/2002jd002587, 2003.

713 Sprenger, M., Wernli, H. and Bourqui, M.: Stratosphere–troposphere exchange and its relation to
714 potential vorticity streamers and cutoffs near the extratropical tropopause, *Journal of the*
715 *Atmospheric Sciences*, 64(5), 1587–1602, doi:10.1175/jas3911.1, 2007.

716 Stamnes, K., Tsay, S.-C., Wiscombe, W. and Jayaweera, K.: Numerically stable algorithm for
717 discrete-ordinate-method radiative transfer in multiple scattering and emitting layered
718 media, *Applied Optics*, 27(12), 2502, doi:10.1364/ao.27.002502, 1988.

719 Wang, H., Lu, X., Jacob, D. J., Cooper, O. R., Chang, K.-L., Li, K., Gao, M., Liu, Y., Sheng, B.,
720 Wu, K., Wu, T., Zhang, J., Sauvage, B., Nédélec, P., Blot, R. and Fan, S.: Global
721 tropospheric ozone trends, attributions, and radiative impacts in 1995–2017: An integrated
722 analysis using aircraft (IAGOS) observations, ozonesonde, and multi-decadal chemical
723 model simulations, *Atmospheric Chemistry and Physics*, 22(20), 13753–13782,
724 doi:10.5194/acp-22-13753-2022, 2022.

725 Wang, M. and Fu, Q.: Stratosphere-troposphere exchange of Air Masses and ozone
726 concentrations based on reanalyses and observations, *Journal of Geophysical Research:*
727 *Atmospheres*, 126(18), doi:10.1029/2021jd035159, 2021.

728 Waugh, D. W. and Polvani, L. M.: Climatology of intrusions into the tropical upper troposphere,
729 *Geophysical Research Letters*, 27(23), 3857–3860, doi:10.1029/2000gl012250, 2000.

730 White, I. P., Lu, H., and Mitchell, N. J.: Seasonal evolution of the QBO-induced wave forcing
731 and circulation anomalies in the northern winter stratosphere, *Journal of Geophysical*
732 *Research: Atmospheres*, 121, 10,411–10,431, <https://doi.org/10.1002/2015jd024507>, 2016.

733 Williams, R. S., Hegglin, M. I., Jöckel, P., Garny, H. and Shine, K. P.: Air quality and radiative
734 impacts of downward-propagating sudden stratospheric warmings (ssws), *Atmospheric*
735 *Chemistry and Physics*, 24(2), 1389–1413, doi:10.5194/acp-24-1389-2024, 2024.

736 Williams, R. S., Hegglin, M. I., Kerridge, B. J., Jöckel, P., Latter, B. G., and Plummer, D. A.:
737 Characterising the seasonal and geographical variability in tropospheric ozone, stratospheric
738 influence and recent changes, *Atmospheric Chemistry and Physics*, 19(6), 3589–3620,
739 doi:10.5194/acp-19-3589-2019, 2019.

740 World Meteorological Organization (1957). *Meteorology—A three dimensional science: Second*
741 *session of the Commission for Aerology*. WMO Bulletin, IV(4), 134–138.

742 Xia, Y., Xie, F. and Lu, X.: Enhancement of Arctic surface ozone during the 2020–2021 winter
743 associated with the sudden stratospheric warming, *Environmental Research Letters*, 18(2),
744 024003, doi:10.1088/1748-9326/acae0, 2023.

- 745 Xia, Y., Huang, Y. and Hu, Y.: On the climate impacts of upper tropospheric and lower
746 stratospheric ozone, *Journal of Geophysical Research: Atmospheres*, 123(2), 730–739,
747 doi:10.1002/2017jd027398, 2018.
- 748 Xie, J., Hu, J., Xu, H., Liu, S., & He, H. (2020). Dynamic diagnosis of stratospheric sudden
749 warming event in the boreal winter of 2018 and its possible impact on weather over North
750 America. *Atmosphere*, 11(5), 438. <https://doi.org/10.3390/atmos11050438>.
- 751 Zhang, J., Zhang, C., Zhang, K., Xu, M., Duan, J., Chipperfield, M. P., Feng, W., Zhao, S., and
752 Xie, F.: The role of chemical processes in the quasi-biennial oscillation (QBO) signal in
753 stratospheric ozone, *Atmospheric Environment*, 244, 117906,
754 <https://doi.org/10.1016/j.atmosenv.2020.117906>, 2020.
- 755 Ziemke, J. R., Chandra, S. and Bhartia, P. K.: “cloud slicing”: A new technique to derive upper
756 tropospheric ozone from satellite measurements, *Journal of Geophysical Research:*
757 *Atmospheres*, 106(D9), 9853–9867, doi:10.1029/2000jd900768, 2001.